Chapter 2

Scaling test in the quenched approximation

In this chapter we will derive a result that was thought to be almost impossible to reach using the standard Wilson formulation of lattice QCD: we will give *continuum* results (in the quenched approximation) for the pseudo scalar mass $m_{\rm PS}$, the pseudo scalar decay constant $f_{\rm PS}$ and the vector mass $m_{\rm V}$ down to values of the pseudo scalar mass of $m_{\rm PS} = 270$ MeV, a value that is almost a factor of 2 smaller than what could be reached with Wilson fermions so far. This result is visualized in figure 2.1, which we will discuss later in detail. But we mention already now that, while simulations with Wilson fermions [79] – represented by open squares – had to be stopped* at values of $m_{\rm PS} \approx 600$ MeV, our data – represented by open squares – reach with controllable errors down to significantly smaller values of $m_{\rm PS}$. Thus, we can finally enter a region of mass values, where contact to chiral perturbation theory (χPT) can be made, without worrying about lattice artifacts and convergence problems of χPT. The tool that made this possible is mtmQCD, as introduced in section 1.2.4.

However, mtmQCD is still a rather new formulation of lattice QCD and hence we had to ascertain and scrutinize this approach. Most important for our understanding of mtmQCD has been a detailed scaling test, which we performed in a wide range of lattice spacings and quark masses in the quenched approximation. In particular, the range of $m_{\rm PS}$ values has been between 270 and 1200 MeV and the range of lattice spacings between 0.048 and 0.17 fm. We show that indeed lattice artifacts linear in a are absent in physical observables and that residual lattice spacing artifacts are small at *all* these values of $m_{\rm PS}$. We perform then continuum extrapolations for the pseudo scalar decay constant and the vector mass finding full agreement with

*In the literature one can find also simulations with Wilson fermions and smaller values of the pseudo scalar mass (cf. for instance [80]). However, in those simulations single, so-called exceptional configurations had to be removed from the ensemble "by hand".

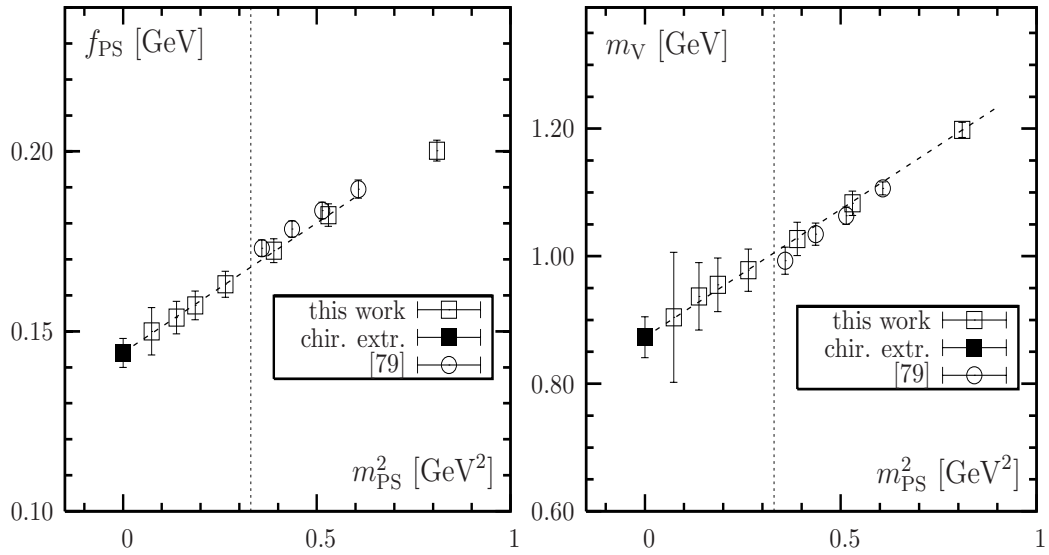

(a) Continuum values of $f_{\rm PS}$ as a function of $m^2_{\rm PS}$.

(b) Continuum values of $m_{\rm V}$ as a function of $m^2_{\rm PS}$.

Figure 2.1: Continuum values of $f_{\rm PS}$ [GeV] (a) and $m_{\rm V}$ [GeV] (b) as a function of $m^2_{\rm PS}$ [GeV^2] and the chiral extrapolation of our data. In addition to our results, represented by squares, we also plot continuum results extracted from data published in [79] where non-perturbatively $\mathcal{O}(a)$ improved Wilson fermions were used. For the chiral extrapolation we used only our results and we indicate the linear extrapolation by the dashed lines. The dotted vertical lines roughly mark the value of $m_{\rm PS}$ where simulations with Wilson fermions had to be stopped.

results available in the literature. In addition we address the important question about size and scaling behavior of flavor breaking effects in mtmQCD, which vanish as a^2, while being non-negligible of size.

Moreover, we compare at one value of the lattice spacing mtmQCD with the overlap formulation of lattice QCD, the latter of which has exact chiral symmetry at finite values of the lattice spacing a, as explained in section 1.2.2. We show that for all the quantities investigated here both formulations reveal consistent results. In particular, it is possible to simulate with both formulations pseudo scalar masses lower than 300 MeV without practical problems. However, a cost comparison yields that the overlap formulation is a factor of 20 to 70 more expensive than mtmQCD.

2.1 The definition of the critical mass

Naturally, when a new formulation is under investigation there are a lot of subtleties to understand and to learn. One of those in case of mtmQCD is the definition of the critical mass, whose potential influence on the cut-off effects will be discussed in the following section. However, beforehand we would like to stress the following remarks:

the proof of $\mathcal{O}(a)$ improvement for mtmQCD is based on the Symanzik effective theory [12, 13, 14], implying that the proof is only valid if the Symanzik expansion itself is valid. In particular, the lattice spacing should be sufficiently smaller than the physical scale. Moreover, since the Symanzik expansion is a perturbative concept, it is assumed that the dependence of quantities under investigation on the lattice spacing is smooth. Especially, in the vicinity of a dis-continuous phase transition – as we will find in the case of dynamical twisted mass fermions in chapter 4 – we cannot expect the expansion to hold.

The only parameter that needs to be tuned in tmQCD in order to obtain $\mathcal{O}(a)$ improvement is the twist angle. Maximal twist is achieved by tuning the angle to a value of $\pi/2$, which is equivalent to setting the value of κ to its critical value κ_{crit} (1-30), or equivalently the value of the (untwisted) bare quark mass m_0 to its critical value m_{crit}. In other words, we are interested in a situation where the renormalized quark mass is determined *only* by the twisted mass $m_{\text{R}} \sim \mu$, i.e. the twisted mass term determines physics. However, any lattice determination of κ_{crit} is affected by errors, which in turn means that the (untwisted) bare quark mass is zero only up to an error: $m_q = 0 + \delta$. This error can have significant consequences for the $\mathcal{O}(a)$ improvement, which we exemplify in the following. Consider again the renormalized quark mass m_{R} at finite lattice spacing. Neglecting the renormalization factors for a moment, which are of order one, this quantity can be estimated by a combination of the twisted mass parameter μ and the untwisted quark mass m_q to be

$$m_{\text{R}} \sim \sqrt{\mu^2 + m_q^2} = \mu \left(1 + \frac{m_q^2}{2\mu^2} + \mathcal{O}(m_q^4/\mu^4)\right) , \tag{2-1}$$

where the expansion is only valid if $m_q = \delta \ll \mu$. It is evident from Eq. (2-1) that if $\delta \ll \mu$ is fulfilled the residual value of m_q contributes only as a small quadratical correction. On the other hand, if $\delta \ll \mu$ is not fulfilled physics is no longer dominated by the twisted mass term as it should be at maximal twist. Hence, it is important for $\mathcal{O}(a)$ improvement to use a κ_{crit} determination with δ as small as possible.

Note that if $\delta \approx \Delta a + \mathcal{O}(a^2)$ with a coefficient Δ one can always find a value of a keeping μ fixed in physical units, where $\delta \ll \mu$ is fulfilled.

In practice, there are at least two ways to determine the value of κ_{crit}: the first is to determine the value of κ where the value of am_{PS} vanishes with pure Wilson fermions, i.e. $\mu = 0$. We will refer to this determination method as the *pion definition* of κ_{crit} and denote it with $\kappa_{\text{crit}}^{\text{pion}}$. This determination involves an extrapolation of $(am_{\text{PS}})^2$ in κ to the κ value where am_{PS} vanishes. The extrapolation contains usually a large uncertainty because simulations with pure Wilson fermions and small pseudo scalar masses are hardly possible and therefore, one has to extrapolate from rather large masses. Unfortunately, the size of the extrapolation error is unknown and cannot easily be parameterized in terms of the lattice spacing.

β	5.7	5.85	6.0	6.1	6.2	6.45
r_0/a	2.924	4.067	5.368	6.324	7.360	10.41
$L^3 \times T$	$14^3 \times 28$	$16^3 \times 32$	$16^3 \times 32$	$20^3 \times 40$	$24^3 \times 48$	$32^3 \times 64$
$N_{\rm meas}^{\rm pion}$	600	378	387	300	260	182
$N_{\rm meas}^{\rm PCAC}$	600	500	400	-	300	-

Table 2.1: For the six values of β this table contains the vlaue for r_0/a, the lattice size and the number of measurements $N_{\rm meas}^{\rm pion}$ with the pion definition and $N_{\rm meas}^{\rm PCAC}$ with the PCAC definition of $\kappa_{\rm crit}$.

The second definition of $\kappa_{\rm crit}$ we consider here makes use of the PCAC relation: At fixed non-zero value of the twisted mass parameter μ the value of κ needs to be determined where the value of $m_\chi^{\rm PCAC}$ vanishes. The resulting value $\kappa_{\rm crit}(a\mu)$ is still depending on the value of μ. This dependence can be removed by extrapolating $\kappa_{\rm crit}(a\mu)$ to $a\mu = 0$. The extrapolation is only short in μ since simulations with a twisted mass parameter can be safely performed also with small values of $a\mu$ and therefore the extrapolation error is assumed to be small. We will refer to this definition of $\kappa_{\rm crit}$ as the *PCAC definition* and denote it with $\kappa_{\rm crit}^{\rm PCAC}$. Note that one main difference between the two definitions is that for $\kappa_{\rm crit}^{\rm pion}$ pure Wilson fermions are used, while for $\kappa_{\rm crit}^{\rm PCAC}$ the tmQCD regularization is used.

In this chapter we will use both of the two definitions for $\kappa_{\rm crit}$ and compare the residual lattice artifacts in physical observables between the pion definition and the PCAC definition for various values of the quark mass and the lattice spacing.

We remark here that the "optimal" definition of $\kappa_{\rm crit}$ with respect to $\mathcal{O}(a)$ improvement with mtmQCD is theoretically not yet clarified. Nevertheless, a detailed discussion of lattice artifacts of mtmQCD can be found in Ref. [45]. In fact, it was shown in this reference that in the Symanzik expansion of an operator O at maximal twist there appear at order a^2 terms proportional to $1/m_{\rm PS}^4$, which are called *leading "infra-red divergent" cut-off effects*. These terms will be strongly visible as large $\mathcal{O}(a^2)$ cut-off effects in the limit of vanishing pseudo scalar masses. In the same reference it was shown that with the PCAC definition of $\kappa_{\rm crit}$ the coefficients multiplying the $(a/m_{\rm PS}^2)^2$ terms vanish faster in the chiral limit than $1/m_{\rm PS}^4$ curing such the problem of those large cut-off effects. Note that in Refs. [81, 82] the same proposal was made, including also arguments from χPT. For a recent discussion see also Refs. [83, 84].

2.2 Scaling test set-up

In order to verify the prediction of Ref. [42] of $\mathcal{O}(a)$ improvement at $\omega = \pi/2$ we have chosen up to six values of the bare coupling constant β in a range of lattice spacing between 0.048 fm and 0.17 fm. We used the Wilson plaquette gauge action (1-25) and periodic boundary conditions for gauge and fermion fields. The β values can be found together with the values for r_0/a and the lattice sizes in table 2.1. The number of measurements $N_{\rm meas}$ for the two $\kappa_{\rm crit}$ definitions can also be found in table 2.1. We have set the Wilson parameter to $r = 1$ and used $r_0 = 0.5$ fm to set the scale throughout this chapter.

In order to fix the physical situation in our scaling test, we decided to study physical quantities as a function of β (i.e. as a function of a) for fixed values of $r_0 m_{\rm PS}$. For this purpose we roughly fixed the values of $r_0\mu$ at each β value to $r_0\mu \approx 0.02, 0.04, 0.08, 0.16, 0.24, 0.32, 0.40$. For the PCAC definition we have two additional intermediate values $r_0\mu \approx 0.059$ and $r_0\mu \approx 0.123$. Note that at $\beta = 6.45$ we have simulated only the two lightest quark masses with the pion definition in order to check our continuum extrapolations.

Due to the wide range of twisted mass values at each β value we could then interpolate the results when necessary to match a desired value of $r_0 m_{\rm PS}$. For the quantities we considered here it was sufficient to perform a linear interpolation in $(r_0 m_{\rm PS})^2$ between the two closest points. We used the ROOT and MINUIT packages from CERN (cf. [85, 86]) for these interpolations. Since we do not want to extrapolate to mass values where we have no data available, the lowest value of the pseudo scalar mass was 298 MeV with the pion definition of $\kappa_{\rm crit}$ and 270 MeV with the PCAC definition.

Since in this chapter we work in the quenched approximation the gauge configurations do not depend on the bare quark masses. We produced at each value of β an ensemble of gauge configurations using a combination of the over-relaxation and the heat-bath algorithm. One heat-bath sweep was always followed by $L/2 + 1$ over-relaxation sweeps, where L is the spatial lattice size. We skipped as many intermediate configurations as needed to obtain completely independent configurations.

Again, because the configuration at each β value are quark mass independent, we could make use of a multi mass conjugate gradient (CG-M) iterative solver as explained in appendix B.2. Such a solver allows one to invert on the lowest mass and get within the same inversion also the result for all the other masses. At $\beta = 6.45$, however, we used even/odd preconditioning, since we simulated only the two lowest values of $r_0\mu$. This preconditioning accelerates the solvers, but prevents us to use a multi mass solver.

In order to compute the quark propagators needed in the contraction of the correlation functions, the Dirac operator needs to be inverted on a given source.

	$am_{\rm PS}$			
$a\mu$	$12^3 \times 24$	$14^2 \times 32$	$16^3 \times 32$	$am_{\rm PS}L\vert_{(L=16)}$
0.005	-	-	0.1700(25)	2.7
0.01	0.2327(70)	0.2301(37)	0.2254(19)	3.6
0.02	0.3193(48)	0.3175(30)	0.3122(16)	5.0
0.04	0.4520(40)	0.4506(23)	0.4452(14)	7.1
0.06	0.5596(35)	0.5575(19)	0.5535(12)	8.9
0.08	0.6541(31)	0.6510(17)	0.6488(11)	10.4
0.10	0.7417(26)	0.7378(16)	0.7359(11)	11.8

Table 2.2: Values of $am_{\rm PS}$ at $\beta = 5.85$ for three different lattice Volumes: $12^3 \times 24$, $14^2 \times 32$ and $16^3 \times 32$. In the last column we also give the value of $am_{\rm PS}L$ for the $16^3 \times 32$ lattice.

The simplest choice here is to use a point source located at $x = 0$ and for every combination of color and spinor indices. Therefore, 12 inversions are needed per configuration. We used a point source for all the results with the pion definition of $\kappa_{\rm crit}$. However, it is known that the overlap with the ground state can be improved if (sink) smearing techniques are applied, which turned out to be crucial in order to determine a reliable estimate for the vector meson mass $m_{\rm V}$. We used Jacobi sink smearing [87] for the determination of $m_{\rm V}$ with the PCAC definition of $\kappa_{\rm crit}$. Since we did not use smearing techniques with the pion definition, we were not able to reliably extract values for $am_{\rm V}$ in this case.

2.2.1 Finite volume effects

Before presenting the results of the scaling test, we show in this subsection results at one value of $\beta = 5.85$ for three different lattice volumes in order to check for finite volume effects. At this value of β we have performed 140 measurements on a $12^3 \times 24$ lattice, 140 measurements on a $14^3 \times 32$ lattice and 380 measurements on a $16^3 \times 32$ lattice, corresponding to physical spatial extends of about 1.48 fm, 1.72 fm and 1.96 fm, respectively. The hopping parameter was set to its critical value $\kappa_{\rm crit}^{\rm pion} = 0.161662(17)$ obtained with the pion definition of $\kappa_{\rm crit}$. We measured the values of the pseudo scalar mass for all three volumes and collected the data in table 2.2.

Aiming for an analysis along the lines of Ref. [88], we first extrapolated the pseudo scalar masses to $L = \infty$ by fitting a functional form

$$am_{\rm PS}(L) \ = am_{\rm PS}(L=\infty) + \frac{a_1}{L^{3/2}} \exp\left\{-a_2 am_{\rm PS}(L=\infty)L\right\} \qquad (2\text{-}2)$$

with coefficient a_1 and a_2 to our data. For the three values of $a\mu$ between 0.01 and 0.04 we show the data points together with the fits in figure 2.2(a). From this figure

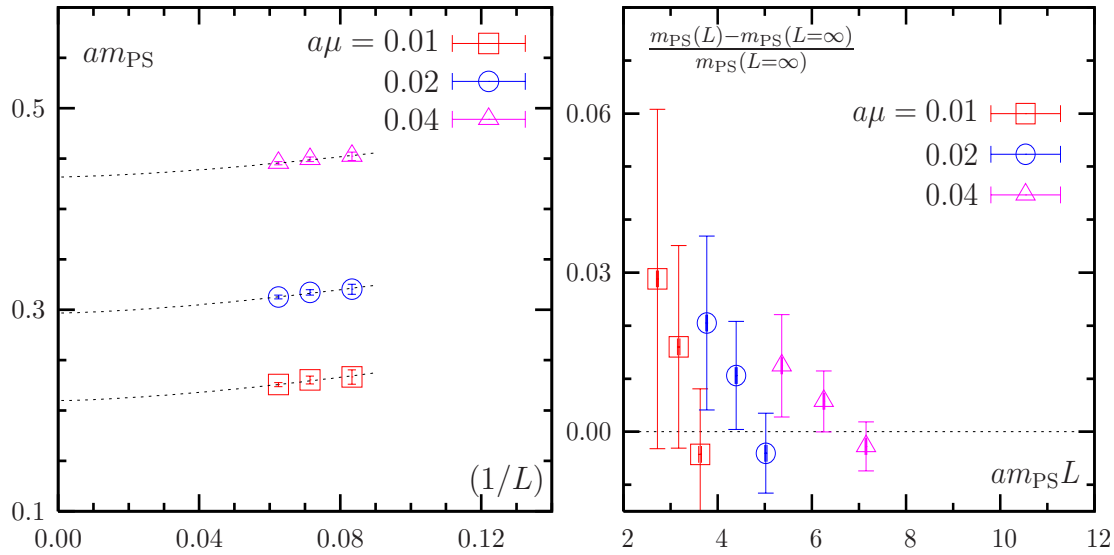

(a) $am_{\rm PS}$ as a function of (a/L).

(b) Relative finite volume effects in $m_{\rm PS}$.

Figure 2.2: Finite volume effects in $m_{\rm PS}$ at $\beta = 5.85$. In (a) $am_{\rm PS}$ is plotted as a function of $(1/L)$ together with exponential fits to the data (see text). In (b) the relative finite volume effects are plotted as a function of $am_{\rm PS}L$. In both graphs we plot only data for the three lowest values of $a\mu$. Note that in our notation L is dimensionless.

it is already evident that finite volume effects, at least for the quantity $am_{\rm PS}$ are small. An analysis of $(m_{\rm PS}(L) - m_{\rm PS}(L = \infty))/m_{\rm PS}(L = \infty)$ (see figure 2.2(b)) shows that for the simulation points corresponding to the smallest values of $a\mu$ the finite volume effects are within $2 - 3$ percent and at most within two standard deviations from the extrapolated infinite volume limit. In practice they are thus not relevant for the following discussion.

Other quantities than $m_{\rm PS}$ are affected by finite volume artifacts of qualitatively the same form as Eq. (2-2) with, of course, in general different coefficients. However, since for the following scaling test we will stay at almost constant physical volume for all values of β under investigation, the scaling test itself should not be affected by finite volume effects.

2.3 Scaling test of mtmQCD

In this section we present the numerical results of the scaling test. We first compare the scaling behavior for the two definitions of $\kappa_{\rm crit}$, present then continuum results for $f_{\rm PS}$ and $m_{\rm V}$ and investigate the flavor breaking effects. Finally, we compare the twisted mass and the overlap formulation.

β	$\kappa_{\rm crit}^{\rm pion}$	$\kappa_{\rm crit}^{\rm PCAC}$
5.7	0.169198(48)	0.171013(160)
5.85	0.161662(17)	0.162379(93)
6.0	0.156911(35)	0.157409(72)
6.1	0.154876(10)	-
6.2	0.153199(16)	0.153447(32)
6.45	0.150009(11)	-

Table 2.3: Values of $\kappa_{\rm crit}^{\rm pion}$ and $\kappa_{\rm crit}^{\rm PCAC}$ for all values of β.

2.3.1 Scaling of the pseudo scalar decay constant with the pion definition of $\kappa_{\rm crit}$

At all the β values of our simulations we made our own determination of the value of $\kappa_{\rm crit}^{\rm pion}$ from the intercept in κ at zero pseudo scalar mass. The values of $\kappa_{\rm crit}^{\rm pion}$ are given in table 2.3. In a first step we then computed the values of $am_{\rm PS}$ at each of our simulation points. The values can be found in table C.1 in appendix C.

Since we work at maximal twist at each value of β we can extract the pseudo scalar decay constant $f_{\rm PS}$ as explained in section 1.3 Eq. (1-84). This prescription allows the extraction of $f_{\rm PS}$ without the need to compute renormalization constants. The results are collected in table C.2 and they are visualized in figure 2.3, where we show $r_0 f_{\rm PS}$ as a function of $(a/r_0)^2$. The different symbols correspond from top to bottom to about $m_{\rm PS} = 720$ MeV, 515 MeV, 380 MeV and 300 MeV. In addition to our data represented by the open symbols we also plot our continuum extrapolation represented by filled symbols (for better visibility some points are slightly displaced). For the continuum extrapolations we used only the data for $\beta \geq 6.0$.

For the interpretation of figure 2.3 it is important to remind that – since we use a multi mass solver – the results at one lattice spacing for different masses are strongly correlated, which explains the similar fluctuations at fixed a/r_0 for the different values of $r_0 m_{\rm PS}$. First of all it is evident from figure 2.3 that for all values of $r_0 m_{\rm PS}$ plotted the cut-off effects are linear in $(a/r_0)^2$ for lattice spacings lower than a given bound. From figure 2.3 we can estimate this bound to be $(a/r_0)^2 < 0.04$. The slope of the continuum extrapolation, however, is strongly mass dependent: it becomes steeper the lower the pseudo scalar mass value becomes. This can only be explained with a dependence of the $\mathcal{O}(a^2)$ cut-off effects on the mass as described in Ref. [45]. The size of these cut-off effects can be significantly reduced by using the PCAC definition of $\kappa_{\rm crit}$, as will be shown in the following subsections.

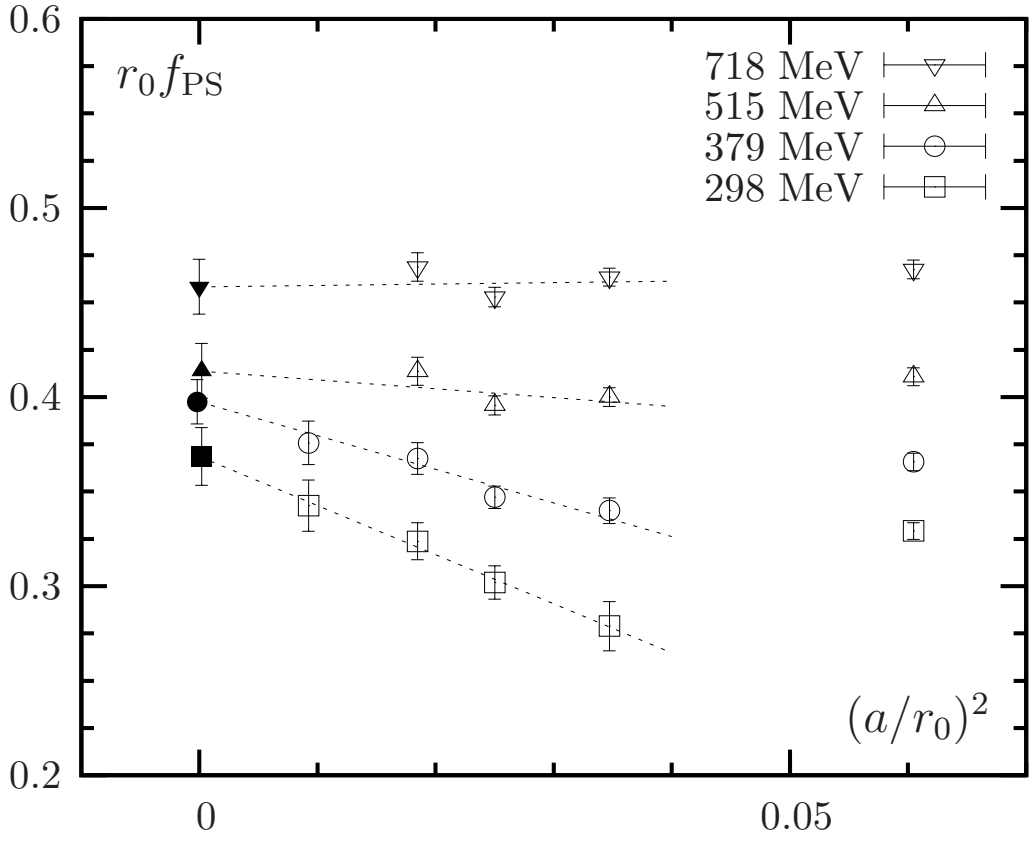

Figure 2.3: Scaling plot for $r_0 f_{\rm PS}$ as a function of $(a/r_0)^2$ for four different values of $r_0 m_{\rm PS}$. The different symbols correspond from top to bottom to 718 MeV, 515 MeV, 379 MeV and 298 MeV. Our data points are represented by open symbols while the continuum extrapolations are plotted with filled symbols

2.3.2 Critical mass from the PCAC relation

With the PCAC definition we considered only the β values 5.7, 5.85, 6.0 and 6.2. At each of these β values we first determined the values of $\kappa_{\rm crit}^{\rm PCAC}$ with the method explained above and collected them in table 2.3. An example for this determination at $\beta = 5.7$ can be found in figure 2.4, where we show in the left panel the interpolation in $1/\kappa$ to the point where $m_\chi^{\rm PCAC} = 0$ and in the right panel the extrapolation of $\kappa_{\rm crit}(a\mu)$ to $a\mu = 0$. With the straight line we indicate the linear extrapolation to $a\mu = 0$ and in addition we included the value of $\kappa_{\rm crit}$ determined by the pion definition in the figure. The difference is supposed to be of $\mathcal{O}(a)$. The errors on the values of $\kappa_{\rm crit}^{\rm PCAC}$ in table 2.3 stem from the necessary inter- and extrapolation.

The first quantity we investigated was again the pseudo scalar meson mass $m_{\rm PS}$. The data are collected in table C.3 in appendix C. In figure 2.5(a) $(am_{\rm PS})^2$ is plotted as a function of $a\mu$ at $\beta = 6.0$ for the two definitions of $\kappa_{\rm crit}$. The data points for the PCAC definition show a linear behavior in $a\mu$ down to very small bare quark masses, which is not observed with the pion definition of $\kappa_{\rm crit}$. This effect is better

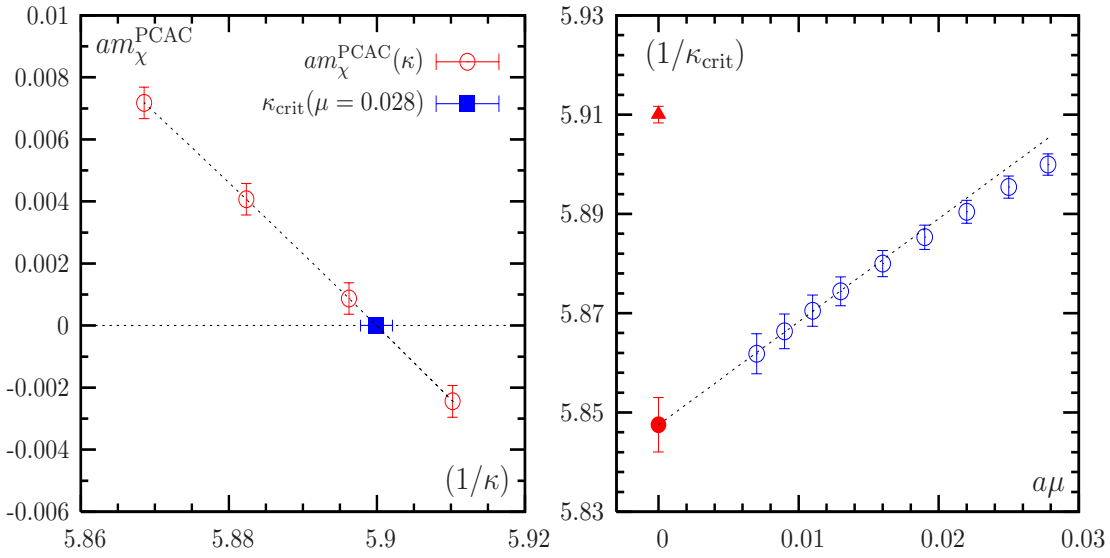

(a) Interpolation in $1/\kappa$. (b) Extrapolation in $a\mu$.

Figure 2.4: Determination of the critical hopping parameter from the PCAC definition at $\beta = 5.7$: (a) interpolation of $am_\chi^{\rm PCAC}(1/\kappa)$ to $m_\chi^{\rm PCAC} = 0$ for one value of the twisted mass parameter $a\mu = 0.028$ (b) $1/\kappa_{\rm crit}$ versus $a\mu$, extrapolation to $a\mu = 0$, the triangle indicates the $1/\kappa_{\rm crit}$ value determined by $(am_{\rm PS})^2 \to 0$ at $\mu = 0$ for unimproved Wilson fermions.

visible in figure 2.5(b), where we plot $(am_{\rm PS})^2/(a\mu)$ as function of $a\mu$. The same behavior is observed for the other β values. This shows that the GMOR relation [89] on the lattice

$$m_{\rm PS}^2 = \mu \frac{2|\langle 0|P|\pi\rangle|^2}{\Sigma} + \mathcal{O}(a^2) \ , \tag{2-3}$$

is not affected by large cut-off effects (see Ref. [45]) when the PCAC definition is used for the determination of $\kappa_{\rm crit}$. Relation (2-3) can be derived from a vector variation of the charged pseudo scalar density, similar to the pure Wilson case [90]. It allows the extraction of the scalar condensate Σ with the need of only the renormalization factor $Z_P = 1/Z_\mu$. Our determination of Z_P and Σ is ongoing [91].

2.3.3 Scaling of $f_{\rm PS}$ with the PCAC definition of $\kappa_{\rm crit}$

As a next quantity we determined $f_{\rm PS}$ from the data with the PCAC definition of $\kappa_{\rm crit}$. The values can be found in table C.4 in appendix C. In order to compare to the results obtained with the pion definition we had to match the values of $r_0 m_{\rm PS}$ by interpolating our results.

First of all, for all our values of $r_0 m_{\rm PS}$ the observed cut-off effects in $f_{\rm PS}$ are linear in $(a/r_0)^2$. Moreover, if we consider at several values of $r_0 m_{\rm PS}$ the size of the $\mathcal{O}(a^2)$ cut-off effects, we find that with the PCAC definition of $\kappa_{\rm crit}$ their size is significantly reduced for small values of $r_0 m_{\rm PS}$ when compared to the pion definition.

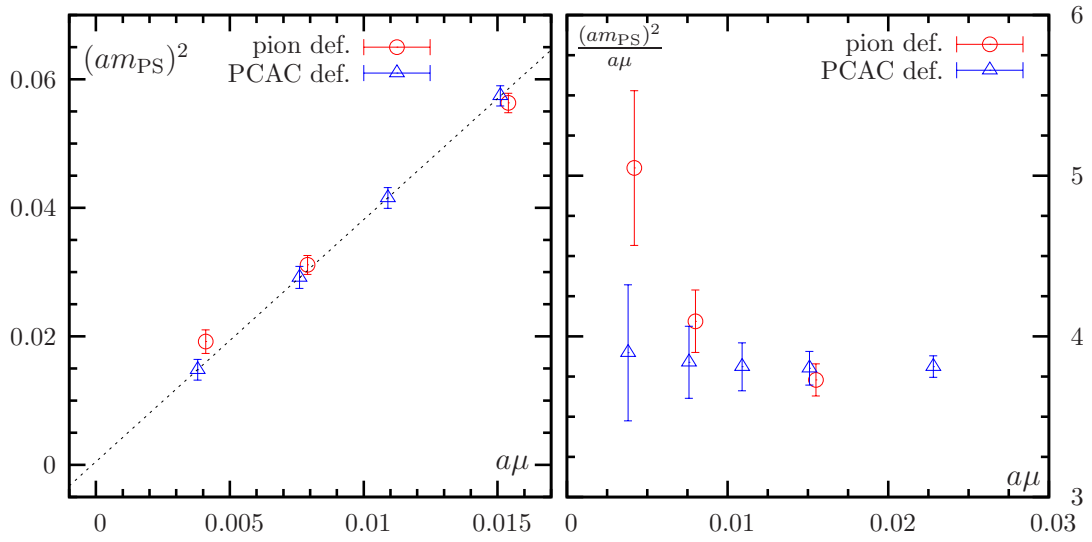

(a) $(am_{\rm PS})^2$ as function of $a\mu$. (b) $(am_{\rm PS})^2/(a\mu)$ as function of $a\mu$.

Figure 2.5: (a) Pseudo scalar mass squared as a function of $a\mu$ both, for the pion definition and the PCAC definition of $\kappa_{\rm crit}$ at $\beta = 6.0$. (b) $(am_{\rm PS})^2/(a\mu)$ for both $\kappa_{\rm crit}$ definitions as function of $a\mu$ at the same value of β. The pion definition data are in (a) and (b) slightly displaced for better visibility.

For the values of $m_{\rm PS} = 298$ MeV and $m_{\rm PS} = 515$ MeV we have plotted $f_{\rm PS}$ in figure 2.6 as a function of $(a/r_0)^2$ for both definitions of $\kappa_{\rm crit}$. It is evident that down to a pseudo scalar mass of 298 MeV the extrapolation of the PCAC definition data is essentially flat. Moreover, the continuum values extrapolated separately for the pion definition and the PCAC definition data agree very well within the errors.

As expected, at small values of the pseudo scalar mass the size of the residual cut-off effects is significantly smaller if the PCAC definition is used instead of the pion definition.

2.3.4 Scaling of the vector meson mass with the PCAC definition of $\kappa_{\rm crit}$

The second quantity we used to check the prediction of automatic $\mathcal{O}(a)$ improvement is the vector mass $m_{\rm V}$. At maximal twist this mass can be extracted from the exponential fall of the two point correlation function C_{AA} or C_{TT} in the twisted basis as explained in section 1.3. The extraction of a value for $m_{\rm V}$ is difficult without smearing techniques, which is in particular the case for small quark masses. Therefore, we used local source and Jacobi smeared sinks to extract the vector meson mass. In addition it turned out that the tensor correlator systematically shows smaller statistical fluctuations and thus, we used exclusively the tensor correlator for the determination of values for $am_{\rm V}$. As explained above we have for $m_{\rm V}$ only

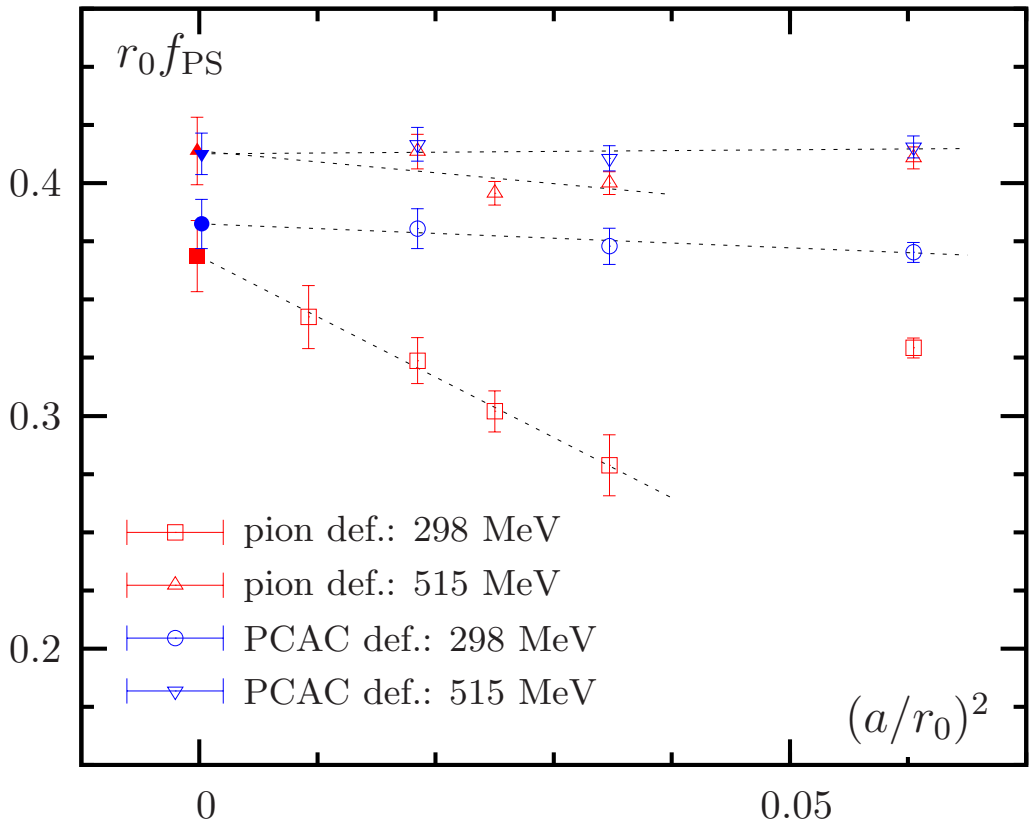

Figure 2.6: Scaling plot for $r_0 f_{\rm PS}$ as a function of $(a/r_0)^2$ for $m_{\rm PS} = 298$ MeV (open circles and open squares) and $m_{\rm PS} = 515$ MeV (open triangles and open inversed triangles). The data points are represented by open symbols while the continuum extrapolations are plotted with filled symbols. Open squares and open triangles represent data obtained with the pion definition of $\kappa_{\rm crit}$, while the open circles and the open reversed triangles represent data obtained with the PCAC definition. The PCAC definition continuum points are slightly displaced for better visibility.

results obtained with the PCAC definition of $\kappa_{\rm crit}$.

The values for $am_{\rm V}$ for all our simulation points with the PCAC definition can be found in table C.5. In fig. 2.7 we show our results for the vector meson mass as a function of $(a/r_0)^2$ for values of $m_{\rm PS} = 900$ MeV, 730 MeV and 270 MeV. As observed for $f_{\rm PS}$, the continuum extrapolations for $m_{\rm V}$ are essentially flat down to pseudo scalar masses of 270 MeV for $(a/r_0)^2 \leq 0.06$, confirming again the expected $\mathcal{O}(a)$ improvement with mtmQCD.

2.3.5 Continuum extrapolation

The continuum extrapolated values of the pseudo scalar decay constant and the vector mass for nine values of $m_{\rm PS}$ are summarized in table C.6. The values quoted there have been extracted only from the data obtained with the PCAC definition, because

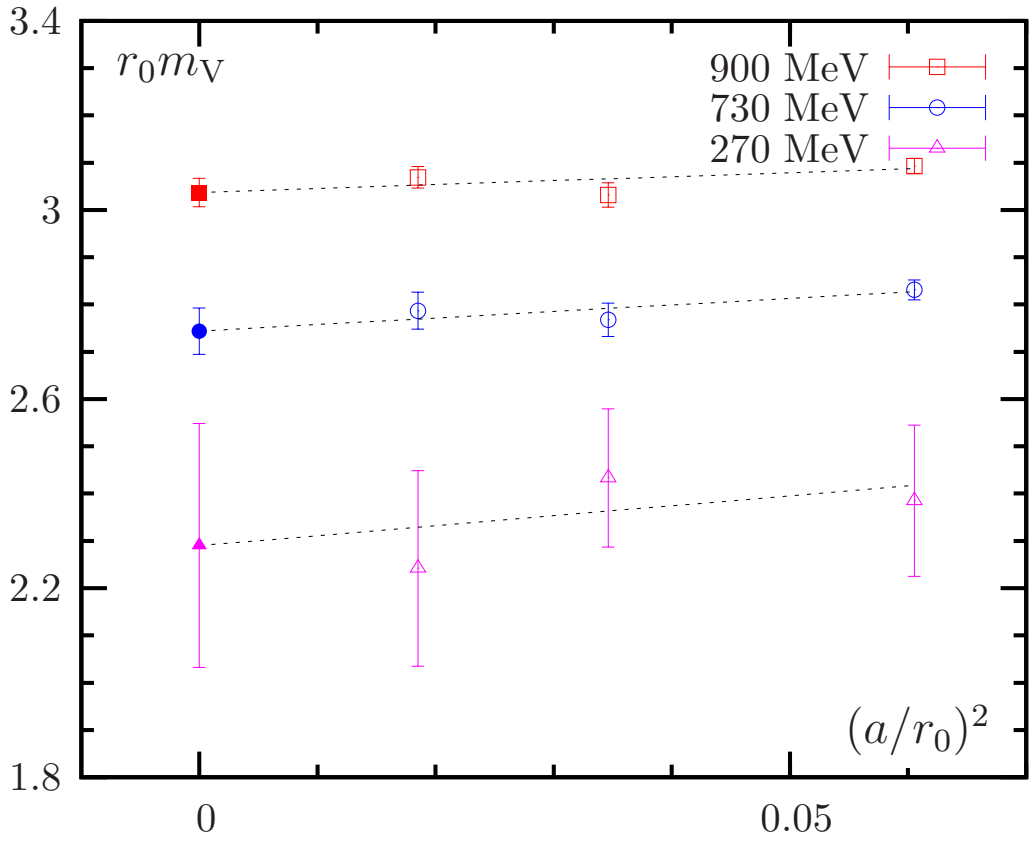

Figure 2.7: $r_0 m_V$ as a function of $(a/r_0)^2$ for three values of $r_0 m_{PS}$ with the PCAC definition of κ_{crit}.

they show much less residual lattice artifacts and the continuum extrapolations are thus more reliable.

In the figures 2.1(a) and 2.1(b), which can be found at the beginning of this chapter, we plot the continuum values of f_{PS} and m_V as functions of m_{PS}^2 in physical units. As a comparison we also plot continuum values that we extracted from the data presented in Ref. [79] where non-perturbatively $\mathcal{O}(a)$ improved Wilson fermions have been used. Both quantities show a linear behavior in the pseudo scalar mass squared without signs of artifacts as predicted from quenched chiral perturbation theory (proportional to $\log a$). Moreover, our results fully agree with the results extracted from Ref. [79], at least for the large values of m_{PS} where a comparison is possible. We extrapolated our results linearly to the chiral limit which is indicated by the dashed lines in the two panels of figure 2.1. The values for f_{PS} and m_V in the chiral limit are collected in table 2.4 together with the values of f_π, m_ρ, f_K and m_{K^*} (the last two in the $SU(3)$ symmetric limit). They were obtained either through the extrapolation to the chiral point (chiral limit, f_π, m_ρ), or by an interpolation (f_K, m_{K^*}).

The ratio $f_K/f_\pi = 1.11(5)$ is 10% smaller than the experimentally obtained

$m_{\rm PS}$ [GeV]	$f_{\rm PS}$ [GeV]	$m_{\rm V}$ [GeV]	
0.0	0.144(4)	0.873(32)	chiral limit
0.137	0.145(4)	0.880(32)	(f_π, m_ρ)
0.495	0.162(5)	0.971(34)	$(f_{\rm K}, m_{\rm K^*})$

Table 2.4: $f_{\rm PS}$ and $m_{\rm V}$ in the continuum (PCAC definition). The values are obtained from a linear fit on the smallest 4 masses (5 in the case of $m_{\rm V}$) and correspond to: the values in the chiral limit (first row); f_π and m_ρ (second row); $f_{\rm K}$ and $m_{\rm K^*}$ in the $SU(3)$ symmetric limit (third row).

values. This deviation is, however, consistent with what was observed in previous quenched calculations [92, 80]. Moreover, the values of m_ρ and $m_{\rm K^*}$ turn out to be $10-15\%$ larger than the experimental values again consistent with other quenched calculations [80].

2.3.6 Flavor breaking effects

As mentioned in section 1.2.4 the flavor chiral rotation to the twisted basis is in the continuum only a formal transformation that leaves the theory invariant. Therefore, even if flavor symmetry seems to be broken in the twisted basis, in the continuum it is only replaced by a modified, but equivalent flavor symmetry. This is not longer true at finite lattice spacing where the flavor symmetry is explicitly broken and only restored in the continuum limit. This manifests itself for instance as a non-vanishing difference of the charged $m_{\rm PS^+}$ and the neutral $m_{\rm PS^0}$ pseudo scalar masses, which is expected to vanish towards the continuum as a^2. It is an important question whether this expectation proves true in practice.

If we consider the local bilinears $P^\pm = \bar\chi\gamma_5\frac{\tau^\pm}{2}\chi$ and $P^0 = \bar\chi\chi$ similar to what we explained in section 1.3, we can extract values for $am_{\rm PS^+}$ and $am_{\rm PS^0}$ from the following correlation functions:

$$\begin{aligned} C_{m_{\rm PS^+}}(t) &= a^3\sum_{\mathbf{x}}\langle[P^+(x)P^-(0)]_{\rm con}\rangle\ , \\ C_{m_{\rm PS^0}}(t) &= a^3\sum_{\mathbf{x}}\langle[P^0(x)P^0(0)]_{\rm con} + [P^0(x)P^0(0)]_{\rm disc}\rangle\ . \end{aligned} \tag{2-4}$$

Here we denote with [.] the fermionic contractions only and indicate with the subscripts "con" and "disc" the connected and the disconnected pieces of the correlation function, respectively. For the neutral pseudo scalar mass it is thus in general needed to evaluate the disconnected contribution

$$[P^0(x)P^0(0)]_{\rm disc} = {\rm Tr}\left\{D_{\rm tm}^{-1}\right\}(x)\,{\rm Tr}\left\{D_{\rm tm}^{-1}\right\}(0)\,. \tag{2-5}$$

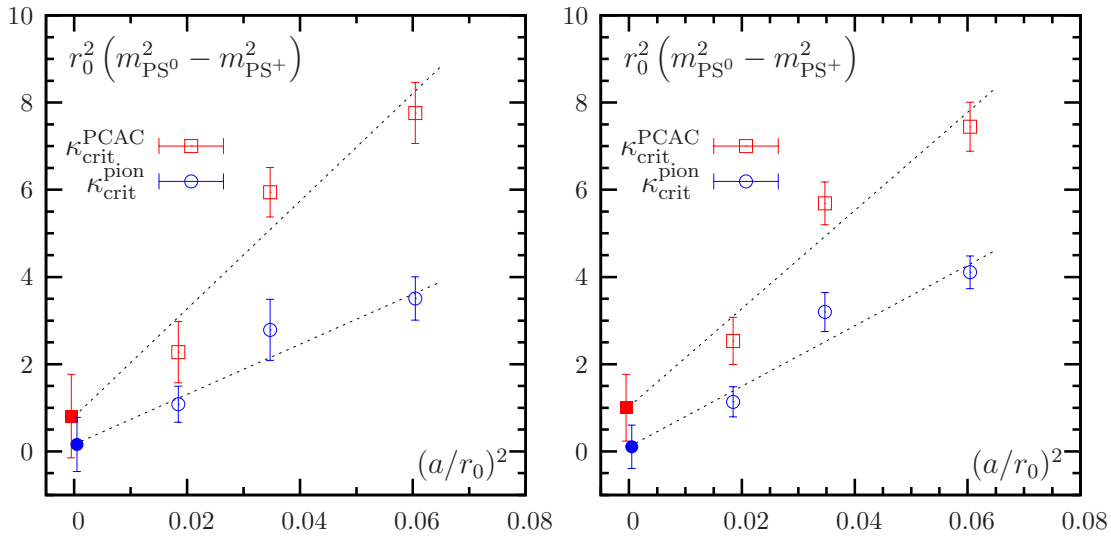

(a) Absolute pseudo scalar mass splitting with $m_{\mathrm{PS}^+} = 298$ MeV.

(b) Absolute pseudo scalar mass splitting with $m_{\mathrm{PS}^+} = 382$ MeV.

Figure 2.8: Absolute pseudo scalar mass difference as a function of $(a/r_0)^2$ for $m_{\mathrm{PS}^+} = 298$ MeV and $m_{\mathrm{PS}^+} = 382$ MeV employing the pion definition and the PCAC definition for the critical point.

with the vacuum contribution to $\mathrm{Tr}\left\{D_{\mathrm{tm}}^{-1}\right\}$ being subtracted and the trace is taken over color and Dirac indices. There are several techniques available to compute those contributions on the lattice, which are mostly based on stochastic estimators and usually rather computer time demanding (see for instance Refs. [93, 94]). However, since we work in the quenched approximation there is a possibility to investigate the aforementioned mass splitting from the connected piece in $C_{m_{\mathrm{PS}^0}}$ only, by reinterpreting the connected piece with the help of the Osterwalder-Seiler (OS) action [95, 96].

The Osterwalder-Seiler action is identical to the twisted mass action, only the τ_3 matrix acting in flavor space is replaced with the unit matrix. Thus, $m_{\mathrm{PS}^+} = m_{\mathrm{PS}^0}$ because flavor symmetry is un-broken and

$$C_{m_{\mathrm{PS}^+}}^{\mathrm{OS}}(t) = C_{m_{\mathrm{PS}^0}}^{\mathrm{OS}}(t)\,. \tag{2-6}$$

The key observation is now that in the quenched approximation, and only in the quenched approximation

$$C_{m_{\mathrm{PS}^0}}^{\mathrm{OS}}(t) = \left(C_{m_{\mathrm{PS}^0}}^{\mathrm{tm}}(t)\right)_{\mathrm{con}}, \tag{2-7}$$

allowing us to interpret $(C_{m_{\mathrm{PS}^0}}^{\mathrm{tm}}(t))_{\mathrm{con}}$ as the correlation function of a local operator. Hence, $(C_{m_{\mathrm{PS}^0}}^{\mathrm{tm}}(t))_{\mathrm{con}}$ has a standard transfer matrix decomposition and the neutral pseudo scalar mass can be extracted from its exponential decay with good precision.

We have extracted values for am_{PS^0} for $\beta = 5.85$, $\beta = 6.0$ and $\beta = 6.2$ with the pion definition and the PCAC definition of κ_{crit}. They can be found in the tables of Ref. [96]. In figure 2.8 we show the mass difference $r_0^2(m^2_{\mathrm{PS}^0} - m^2_{\mathrm{PS}^+})$ as a function of $(a/r_0)^2$ for both definitions of κ_{crit} and for values of $m_{\mathrm{PS}^+} = 298$ MeV and 387 MeV. As expected, the difference vanishes proportional to a^2 and the continuum extrapolated values are consistent with zero. However, the mass splitting is not small and in addition its size differs significantly for the two definition of κ_{crit}: the results obtained with the PCAC definition show larger flavor breaking effects. This is at first unexpected, because for all the other quantities used in this scaling test the $\mathcal{O}(a^2)$ artifacts are smaller for the PCAC definition when compared to the pion definition.

Our interpretation for this phenomenon is again based on the symmetries of the twisted mass formulation. With the PCAC definition parity is maximally restored at finite lattice spacing, but at the same time flavor symmetry is maximally broken, which is expressed in chiral perturbation theory in the fact that the mass splitting is proportional to $\sin(\omega)$ [97, 82]. We also remark that the mass splitting $(m_{\mathrm{PS}^0} - m_{\mathrm{PS}^+})$ comes out to be positive which is consistent with the realization of an Aoki phase scenario in the quenched approximation (see chapter 4 for more details).

2.4 Overlap versus twisted mass fermions

In the last section we have demonstrated that with mtmQCD $\mathcal{O}(a)$ improvement can be obtained without the need of any improvement coefficient, which is indeed a big advantage of this lattice QCD formulation. We mentioned in section 1.2.4 that tmQCD has a further advantage compared to the original Wilson formulation: the twisted mass parameter serves as an infra-red regulator for the low lying eigenvalues of the lattice Dirac operator [43]. Therefore, it is possible to perform simulations with pseudo scalar mass of about 270 MeV as we have also shown in the last section.

The tmQCD formulation shares these two properties with the overlap formulation, while the latter has the additional property of exact chiral symmetry on the lattice. All this makes a comparison between the two formulations rather interesting. Unfortunately, as also discussed in section 1.2.2, the overlap formulation is much more computer time demanding than the twisted mass formulation making it impossible for us to repeat the scaling test as presented in the last section with the overlap operator. We could only afford for simulations with the overlap formulation at one value of $\beta = 5.85$ on lattices of size $12^3 \times 24$ (for a first scaling study see [98]). We used the overlap operator as defined in Eq. (1-38) with the parameter $\rho = 1.6$ fixed and bare masses of $am_{\mathrm{ov}} = 0.01, 0.02, 0.04, 0.06, 0.08, 0.10$ matching six values for $a\mu$ for the twisted mass simulations at $\beta = 5.85$. We approximated the inverse

$am_{\rm ov}$	$am_{\rm PS}^{\rm PP-SS}$	$aLm_{\rm PS}^{\rm PP-SS}$	$af_{\rm PS}$	$am_{\rm V}$
0.01	0.140(20)	1.6	0.0934(90)	0.632(34)
0.02	0.196(14)	2.3	0.1012(53)	0.638(26)
0.04	0.280(10)	3.4	0.1060(34)	0.653(16)
0.06	0.346(8)	4.2	0.1106(25)	0.666(12)
0.08	0.401(7)	4.8	0.1157(22)	0.683(09)
0.10	0.451(6)	5.4	0.1209(21)	0.702(08)

Table 2.5: Values for the pseudo scalar mass with the overlap formulation at $\beta = 5.85$ on $12^3 \times 24$ lattices. In addition we provide values for $aLm_{\rm PS}^{\rm PP-SS}$, the pseudo scalar decay constant and vector mass for overlap at $\beta = 5.85$.

square root by means of Chebyshev polynomials to an absolute accuracy of 10^{-15}. In the construction of the polynomial we also project out the lowest 20 eigenvalues of $Q^2 = (\gamma_5 D_{\rm W})^2$. For details on the numerical treatment of the overlap operator see Ref. [99]. With the overlap operator we performed measurements on 140 gauge configurations and extracted values for $am_{\rm PS}$, $af_{\rm PS}$ and $am_{\rm V}$.

The pseudo scalar mass has been extracted from $C_{PP-SS}^{\rm ov}$ (cf. Eq. 1-88). The scalar meson state did not affect the extraction, presumably because the quark masses are small enough to let the pseudo scalar state be dominant at sufficiently small values of t/a. The values for $am_{\rm PS}$ can be found in table 2.5. In addition to these values we provide values for $aLm_{\rm PS}^{\rm PP-SS}$ which we used to estimate the finite volume effects. Given these values of $aLm_{\rm PS}^{\rm PP-SS}$ and the experience from tmQCD, we expect very small finite volume effects for the five heaviest quark masses (again at a level of a few percent). For the lowest mass finite volume effects can be more relevant and therefore we usually do not include the corresponding data points in fits. However, the analysis of the quantities presented below suggests that also for this value of the quark mass $am_{\rm ov} = 0.01$ finite volume effects are not larger than our statistical error.

In figure 2.9 we show the pseudo scalar mass squared as a function of the bare mass $am_{\rm bare}$ for the overlap and the twisted mass formulation at $\beta = 5.85$. For the overlap formulation the bare mass corresponds to $am_{\rm ov}$ while for twisted mass fermions to $a\mu$. For the twisted mass data we took solely the results obtained with the PCAC definition of $\kappa_{\rm crit}$. In addition to our twisted mass and overlap data we show data points obtained with standard $\mathcal{O}(a)$ improved Wilson fermions [100, 101].

From figure 2.9 one can see that at equal value of the bare quark mass the value of $am_{\rm PS}$ is smaller for overlap fermions than for twisted mass fermions. This suggests that the renormalization factor Z_μ of the quark mass is larger for Wilson twisted mass fermions compared to the corresponding factor for overlap fermions. Nevertheless, it is evident that with both formulations values of about $m_{\rm PS} = 270$ MeV can

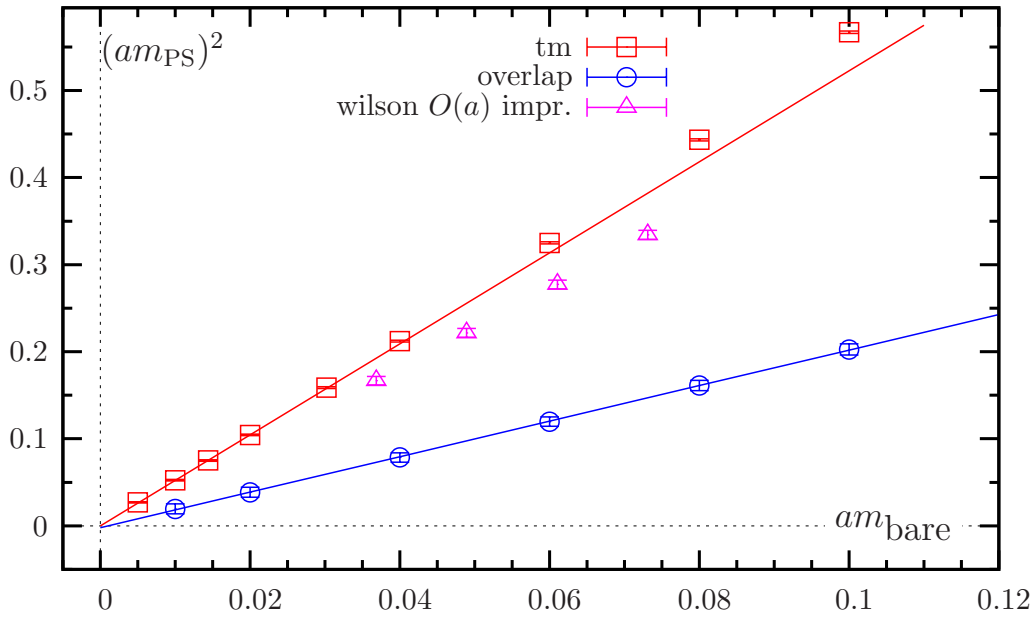

Figure 2.9: Comparison of $am_{\rm PS}^2$ as a function of the bare quark mass between overlap and twisted mass formulation at $\beta = 5.85$. The overlap data are represented by open circles and the twisted mass data by open squares. In addition we plot data from simulations with $\mathcal{O}(a)$ improved Wilson fermions [100, 101]. $m_{\rm bare}$ labels the quark mass corresponding to μ for tmQCD and to $m_{\rm ov}$ the overlap. The solid lines are fits to the twisted mass and the overlap data. While for the fit we used in case of the overlap all the data points, for the twisted mass data we used only the four data points corresponding to the lowest pseudo scalar masses.

be reached without suffering from exceptional configurations. Moreover, for both formulations the squared pseudo scalar mass can be well approximated by a linear function of the bare quark mass down to the smallest mass values. In fact a linear extrapolation to the chiral limit gives in both cases a value for the intercept which is zero within the errors. For the twisted mass data we included only the lowest five masses in the fit, which was not necessary in case of overlap fermions.

In table 2.5 we have also collected the results for $af_{\rm PS}$ and $am_{\rm V}$ for the overlap operator at $\beta = 5.85$. The values for $af_{\rm PS}$ were determined using Eq. (1-93) and hence, do not require any renormalization constant. The vector mass $m_{\rm V}$ was extracted from $C_{VV}^{\rm ov}$ (1-90).

Since we could perform the continuum extrapolation for these two quantities with the twisted mass formulation, we can compare the overlap results at $\beta = 5.85$ on the one hand to twisted mass results at the same β value and on the other hand to the continuum results. The result of this comparison can be found in the four panels of figure 2.10.

In this figure we plot $r_0 f_{\rm PS}$ and $r_0 m_{\rm V}$ as functions of $(r_0 m_{\rm PS})^2$. For the twisted mass results at $\beta = 5.85$ we use solely the data obtained with the PCAC definition

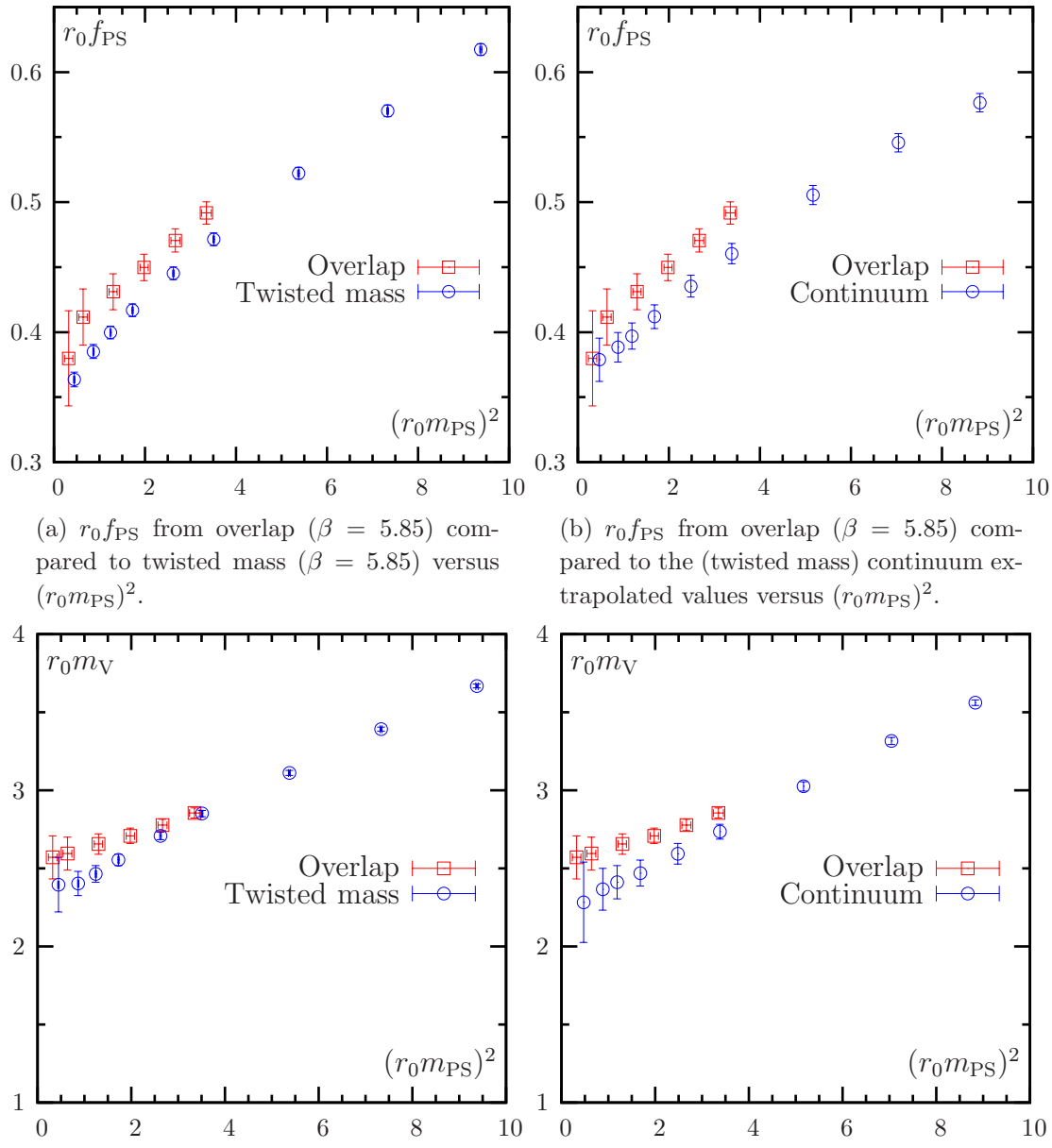

(a) $r_0 f_{\rm PS}$ from overlap ($\beta = 5.85$) compared to twisted mass ($\beta = 5.85$) versus $(r_0 m_{\rm PS})^2$.

(b) $r_0 f_{\rm PS}$ from overlap ($\beta = 5.85$) compared to the (twisted mass) continuum extrapolated values versus $(r_0 m_{\rm PS})^2$.

(c) $r_0 m_{\rm V}$ from overlap ($\beta = 5.85$) compared to twisted mass ($\beta = 5.85$) versus $(r_0 m_{\rm PS})^2$.

(d) $r_0 m_{\rm V}$ from overlap ($\beta = 5.85$) compared to the (twisted mass) continuum extrapolated values versus $(r_0 m_{\rm PS})^2$.

Figure 2.10: Comparison overlap and twisted mass formulation for $f_{\rm PS}$ and $m_{\rm V}$.

of $\kappa_{\rm crit}$. For both quantities a difference between the overlap results and the twisted mass results at finite values of the lattice spacing are visible, as well as between the overlap results and the continuum results. This suggests that the results obtained with the overlap operator are affected by small, but visible $\mathcal{O}(a^2)$ lattice artifacts.

Comparing 2.10(a) with 2.10(b) and 2.10(c) with 2.10(d) it is visible, that the data points for twisted mass at $\beta = 5.85$ and the continuum points are very close to

m_{PS} [MeV]	$a\mu$	am_{ov}
230	0.004	0.01
390	0.0125	0.03
555	0.025	0.06
720	0.042	0.10

Table 2.6: Bare quark masses for the cost comparison between overlap and twisted mass formulation at $\beta = 5.85$.

each other. This indicates again that the $\mathcal{O}(a^2)$ lattice artifacts in these quantities are very small.

2.4.1 Cost comparison

So far we have concentrated in this section on the comparison between the overlap and the twisted mass formulation of lattice QCD on the basis of physical results. We have seen that both the formulations are capable of simulations with pseudo scalar masses lower than 300 MeV. Despite the fact that the overlap formalism provides exact chiral symmetry on the lattice and is thus theoretically best founded for lattice simulations, it seems that twisted mass fermions can serve for many quantities as an equivalent alternative. This becomes even clearer by noting that with dynamical twisted mass fermions and a clever choice of the valence quark discretization mixing of operators with wrong chirality can often be avoided [46]. Thus we are eventually left to decide between the two formulations by means of a cost comparison.

In order to perform a cost comparison between twisted mass and overlap formulation we have chosen a set-up consisting of two quenched ensembles of 20 configurations with $L = T = 12$ and $L = T = 16$, respectively. Both were generated with the Wilson gauge action at $\beta = 5.85$ corresponding to a lattice spacing of $a = 0.12$ fm. We have tuned the bare twisted mass parameter $a\mu$ and the overlap bare quark mass am_{ov} such that the values of the pseudo scalar masses are matched. The actual values can be found in table 2.6.

We then invert the twisted mass and the overlap operator separately on two point-like sources η requiring a stopping criterion of $\|Ax - \eta\| < 10^{-14}$. We are working in the chiral basis (see appendix A.1) and have chosen the two sources to correspond to the two different chiral sectors. The inversions are usually performed with iterative solvers. In order to test the performance of different available solvers, we have implemented the minimal residual (MR), the conjugate gradient normal equation (CG(NE)), the conjugate gradient squared (CGS), the stabilized Bi-conjugate gradient (BiCGstab), the generalized minimal residual (GMRES) (see Ref. [102] for all of them) and the shifted minimal residual (SUMR) (cf. Ref. [103])

iterative solvers. The SUMR method is not applicable to the twisted mass operator, because it requires a shifted unitary operator. Moreover, some of the solvers fail to invert the twisted mass operator or converge only if D_{tm} is multiplied with γ_5.

The computationally most expensive part in the inversion of the overlap operator is the approximation of $(A^\dagger A)^{-1/2}$ in Eq. (1-37), where we use the hermitian Wilson-Dirac operator as kernel $A \equiv Q = \gamma_5 D_{\mathrm{W}}$. As mentioned before the square-root is approximated by means of Chebyshev polynomials, which have an degree of the order $200 - 300$ in our particular set-up, if we project out the lowest 20 and 40 eigenvectors of Q on the 12^4 and 16^4 lattices, respectively. Hence, per application of the overlap operator the Wilson-Dirac operator must be applied order $400 - 600$ times.

One strategy to reduce the number of Q application during the inversion of D_{ov} is to adapt the accuracy of the Chebyshev approximation. This can speed up the inversion by large factors since a reduction in the order of the polynomial enters multiplicatively in the total cost of the inversion. We denote the usage of adaptive precision by a subscript $_{\mathrm{ap}}$ to the solver name. Depending on the solver the adaptive precision was applied in different ways. In case of the $\mathrm{CG}_{\mathrm{ap}}$ we cut the polynomial as soon as the contribution to the resulting vector are smaller than the desired residuum by a factor 10^{-2}. This requires the full polynomial only at the beginning of the CG-search while towards the end polynomials of $\mathcal{O}(10)$ are sufficient. In the case of the $\mathrm{MR}_{\mathrm{ap}}$ or the $\mathrm{GMRES}_{\mathrm{ap}}$ on the other hand it is possible to start with a $\mathcal{O}(10)$ polynomial right at the beginning. From time to time the introduced error is corrected for by calculating the residuum to full precision. This corresponds to a restart of the solver, which is for these two particular solvers a natural procedure.

In the special case of the CG(NM) solver an additional factor of two can be saved when the overlap operator is inverted. Since in the CG(NM) the squared operator $\gamma_5 D_{\mathrm{ov}} \gamma_5 D_{\mathrm{ov}}$ - which is real and positive - is inverted, one can make use of the property of D_{ov} that $P_\pm D_{\mathrm{ov}} P_\pm \propto P_\pm D_{\mathrm{ov}}^\dagger D_{\mathrm{ov}} P_\pm$, where $P_\pm = (1 \pm \gamma_5)/2$ denote the projectors on the positive and negative chiral sector. Therefore, if the sources are chiral half of the applications of D_{ov} can be saved. We denote this algorithm by CG_χ, which can also be combined with adaptive precision $\mathrm{CG}_{\mathrm{ap},\chi}$.

A further way to speed up the inversion of the overlap operator is the so called low mode preconditioning [104], which is supposed to help in the regime of quark masses lighter than what we have used. Therefore, in this chapter we did not include low mode preconditioning in the comparison. While for the overlap operator even/odd preconditioning cannot be applied due to the polynomial approximation of $(Q^\dagger Q)^{-1/2}$, it can be used for the twisted mass operator to reduce the inversion cost. See appendix B.1 for details on how to implement the inversion with even/odd preconditioning.

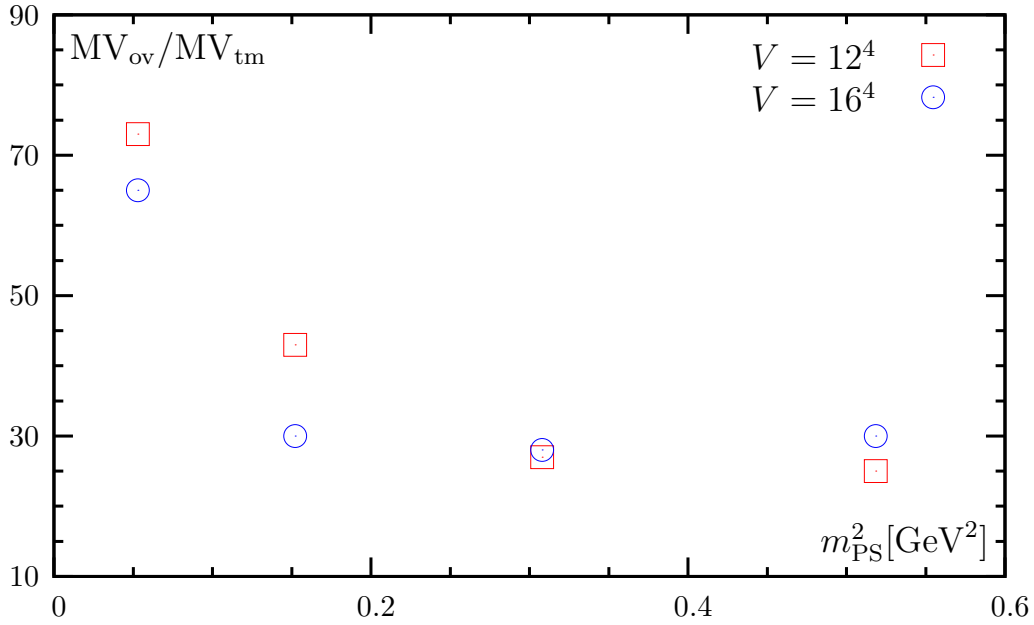

Figure 2.11: $\mathrm{MV_{ov}/MV_{tm}}$ of the fastest available solver versus $m^2_{\mathrm{PS}}[\mathrm{GeV}^2]$ for the two volumes $V = 12^4$ and $V = 16^4$.

We are left to define which quantity we use in the comparison of the different solvers and then also the two different operators. One application of D_{tm} is as expensive as one application of its even/odd preconditioned version as well as one application of the kernel of the overlap operator. Hence, it is natural to use the number of those applications for the comparison. Of course, the different iterative solvers have in general a different amount of additional linear algebra operations, which could be included in the comparison by measuring the wall clock time needed for the inversions. However, the latter measure is highly machine dependent and in addition our experience shows that the number of operator applications (which we will denote by matrix vector (MV) multiplications) is a sufficient criterion.

Our results clearly reveal that in case of the twisted mass operator the CG in combination with even/odd preconditioning is the best choice in the whole range of masses and for both the volumes we investigated here. For the overlap operator the $\mathrm{GMRES_{ap}}$ is the fastest algorithm of the iterative solvers we considered, apart from the simulation point with a 12^4 lattice volume and $m_{\mathrm{PS}} = 230$ MeV where the $\mathrm{CG_{\chi,ap}}$ is the fastest.

For the fastest available solvers we plot in figure 2.11 the ratio of overlap kernel applications $\mathrm{MV_{ov}}$ and applications the preconditioned twisted mass operator $\mathrm{MV_{tm}}$ versus m^2_{PS} in physical units. Depending on the mass and the volume, the inversion of the twisted mass operator is a factor 20 to 70 faster than the inversion of the overlap operator at matched values of the pseudo scalar mass from 230 MeV to 720 MeV. When the two different volumes are compared the overlap operator performs slightly

better on the larger volume when compared to the twisted mass operator. But, of course, for a definite conclusion we would need at least one additional volume.

2.5 Conclusion

In this chapter we presented a detailed scaling test in the quenched approximation of the twisted mass lattice QCD formulation at maximal twist. To this end we have computed several physical quantities in a range of lattice spacings between 0.17 fm and 0.048 fm and pseudo scalar masses between 270 MeV and 1.2 GeV. In order to work at full twist ($\omega = \pi/2$) it is necessary to determine the critical value of the hopping parameter $\kappa_{\rm crit}$. We have explored the pion definition and the PCAC definition for this parameter in order to investigate the influence of these particular choices on the lattice artifacts.

The results of our – quenched – study for the vector meson mass $m_{\rm V}$ and the pseudo scalar decay constant $f_{\rm PS}$ are very encouraging. Our data strongly suggest that in this setup the lattice spacing effects are substantially reduced with respect to standard Wilson fermions and consistent with vanishing $\mathcal{O}(a)$ discretization errors. This holds for both the pion definition and the PCAC definition of $\kappa_{\rm crit}$. Using the PCAC definition of the critical mass the scaling region is found to start already at $(a/r_0)^2 \leq 0.06$ for the observables investigated here, while for the pion definition this region starts only at $(a/r_0)^2 \leq 0.04$. Moreover, the $\mathcal{O}(a^2)$ artifacts remain small for pseudo scalar masses down to 270 MeV when the PCAC definition is used, which is not the case for the pion definition. However, at the two smallest quark masses, we had to include for the pion definition a point at $\beta = 6.45$ in order to safely control the continuum limit extrapolation.

In the case of $f_{\rm PS}$ we have explicitly checked that both definitions of the critical mass lead *independently* to consistent values in the continuum limit. Nevertheless, for further simulations the PCAC definition of κ_c is clearly preferable as it leads to considerably smaller lattice artifacts at small quark masses, allowing at the same time for an enlargement of the scaling region.

We also investigated the flavor breaking effects in the twisted mass formulation. Flavor symmetry is explicitly broken by the twisted mass term at finite values of the lattice spacing. We have shown that the mass splitting between the neutral and the charged pseudo scalar state is not small. But, as expected, the splitting vanishes like a^2 in the continuum limit.

In addition we confronted at one value of the bare coupling constant $\beta = 5.85$ results obtained with the overlap formulation with corresponding results obtained with the twisted mass formulation of lattice QCD. We find that for the quantities investigated in this chapter the two formulations are compatible, in particular

pseudo scalar masses smaller than 300 MeV can be reached with both formulations. However, with a detailed test of various iterative solvers for both formulations we could show that (quenched) simulations with the twisted mass formulation are a factor of 20 to 70 faster than with the overlap formulation, depending on the mass under consideration.

Therefore, the results of this chapter clearly reveal that mtmQCD allows for reliable simulations at pseudo scalar meson masses of about 270 MeV without running into problems with exceptionally small eigenvalues. In addition lattice artifacts linear in a are absent and, when the PCAC definition of the critical mass is used, also the residual lattice artifacts are small in the whole range of masses investigated here. At the same time the costs are significantly less than what is needed for the overlap formulation. In view of future dynamical simulations with light quark masses this is, we think, a very important lesson.